Available online at www.sciencedirect.com

ScienceDirect

Ceramics International 40 (2014) 2249–2260

CERAMICS INTERNATIONAL

www.elsevier.com/locate/ceramint

Optical and dielectric features of zinc oxy fluoro borate glass ceramics with TiO_2 as crystallizing agent

P. Naresh[a], G. Naga Raju[b], V. Ravi Kumar[b], M. Piasecki[c], I.V. Kityk[d,e], N. Veeraiah[a,*]

[a]Department of Physics, Acharya Nagarjuna University, Nagarjuna Nagar, 522 510 A.P., India
[b]Department of Physics, Krishna University, Nuzvid Campus, Nuzvid, 521 201 A.P., India
[c]Institute of Physics, Jan Dlugosz University Czestochowa, Aleja Armii Krajowej 13/15, 42-200 Czestochowa, Poland
[d]Electrical Engineering Department, Czestochowa University of Technology, Aleja Armii Krajowej 17/19, PL-42-201 Czestochowa, Poland
[e]Physical Chemistry Department, Eastern European Univeristy, Voli 6, Lutsk, Ukraine

Received 18 July 2013; received in revised form 20 July 2013; accepted 29 July 2013
Available online 3 August 2013

Abstract

$ZnO–ZnF_2–B_2O_3$ glasses were synthesized and crystallized with different concentrations of TiO_2 (0–0.5 mol% in the steps of 0.1) as nucleating agents. The prepared samples were characterized by XRD, SEM and DSC. These studies have revealed that the samples contain well defined randomly distributed crystalline phases with the complexes of Ti^{4+} and Ti^{3+} ions. Optical absorption studies have indicated that a part of titanium ions exist in Ti^{3+} state in the bulk samples. Dielectric properties were also studied over broad ranges of temperature and frequency of the glass ceramics. The obtained results were analyzed in terms of different polarization mechanisms. The dielectric break down strength of titled glass ceramics was also measured at room temperature in the air medium. The break down strength is found to decrease with the concentration of nucleating agent. The analysis of the results of dielectric properties indicated a decrease of insulating strength of the glass ceramic samples with increase of TiO_2 content.

Keywords: B. Spectroscopy; C. Dielectric properties; D. Glass ceramics

1. Introduction

ZnO imparts a unique combination of optical, electrical and magnetic properties when used in glass matrices like borate. It reduces the coefficient of thermal expansion, imparts high brilliance, luster and high stability against deformation under stress of the glass [1–3] and makes the glasses nontoxic and nonhygroscopic. These features make them very promising candidates for application as laser materials.

The conventional glasses viz., borates, silicates with ZnO as a component posses low specific heat, high thermal conductivity. The dissipation of heat due conduction is more rapid in these glasses when compared with that of glasses containing heavy metal oxide modifiers like BaO and PbO. Because of these characteristics ZnO containing glasses find newer applications such as low-melting glass for metal-to-glass seals, thermistors for use as lighting arresters and devitrified glasses of low thermal expansion. Further, ZnO improves the dielectric strength of the host glass. For this reason thin layers of these glasses are being extensively used as insulating layers in plasma display panels [4,5].

Concerning the optical properties, zinc oxide makes the glass as an outstanding extender for the absorption in the ultraviolet region, it endows direct wide band gap and large exciting binding energy to the host glass. Because of these qualities, glasses containing ZnO are being used for the development of optoelectronic devices, solar energy converters, ultraviolet emitting lasers and gas sensors [6–8]. Further, ZnO based glasses and glass ceramics are good luminescent materials and emit light in the UV and visible regions due to the transition of trapped electrons owing to the intrinsic defects such as oxygen vacancies, oxygen interstitials and zinc interstitials [9]. For these applications, the key property of ZnO is its high electrical conductivity combined with low absorption of visible light [1]. Addition of ZnF_2 to $ZnO–B_2O_3$

*Corresponding author. Tel.: +91 863 2293174.
E-mail address: nvr8@rediffmail.com (N. Veeraiah).

0272-8842/$ - see front matter © 2013 Elsevier Ltd and Techna Group S.r.l. All rights reserved.
http://dx.doi.org/10.1016/j.ceramint.2013.07.143

glass matrix decrease the viscosity and liquidus temperature to a substantial extent [10,11]. Moreover, it is also predicted that, that the presence of compounds like zinc fluoride in the glass matrices, widens the glass-forming region of the system [12].

Partial crystallization of the glasses with appropriate nucleating agent is expected to influence several physical properties i.e., optical, mechanical, electrical, thermal and chemical durability. Transparency of glass after the crystallization can be retained by monitoring the crystallization of a glass precursor with appropriate chemical composition and appropriate nucleating agent. Investigations along these lines have been carried out on several borate, silicate, fluoride or oxy fluoride glass systems [13–16]. The characteristics of glass ceramic depend on the kind and quantity of the crystalline phase formed as well as on the residual glass composition.

Among various crystallizing agents, TiO_2 is expected to be more effective mineralizer especially in the glass systems like $ZnO–ZnF_2–B_2O_3$ when compared with the other nucleating agents. In general, the ions of titanium, exist in the glass in Ti^{4+} state and participate in the glass network forming with different principal polyhedral, viz., TiO_4, TiO_6 and sometimes with TiO_5 (comprising of trigonal bipyramids) structural units [17,18]. The inclusion of Ti^{4+} ions into this glass is an advantage since the empty or unfilled 3d-shells of Ti ions contribute substantially to the non-linear second-order polarizabilities described by the third rank polar tensors. This one allows to produce multi-functional elements for quantum electronics with these glasses. Titanium ions may also exist in Ti^{3+} valence state in glass matrices [19] and expected to influence the physical properties of the glass to a large extent.

In the present investigation we have synthesized $ZnO–ZnF_2–B_2O_3$ glasses, crystallized them with different concentrations of TiO_2 as nucleating agent and characterized them by a variety of techniques viz., XRD, SEM and DSC. Later, we have recorded IR, optical absorption and dielectric dispersion and analyzed the results in order to have some understanding over the influence of titanium valance states and their coordination with oxygen on structural features of the $ZnO–ZnF_2–B_2O_3$ glass ceramics. Such studies may be helpful for considering these glass ceramics for the applications discussed above.

2. Experimental

The detailed compositions of the glasses used in the present study are as follows:

TC_0: $10.0ZnO–30ZnF_2–60B_2O_3$
TC_1: $9.9ZnO–30ZnF_2–60B_2O_3$: $0.1TiO_2$
TC_2: $9.8ZnO–30ZnF_2–60B_2O_3$: $0.2TiO_2$
TC_3: $9.7ZnO–30ZnF_2–60B_2O_3$: $0.3TiO_2$
TC_4: $9.6ZnO–30ZnF_2–60B_2O_3$: $0.4TiO_2$
TC_5: $9.5ZnO–30ZnF_2–60B_2O_3$: $0.5TiO_2$

Among various glass compositions, this range of concentration seems to have formed a relatively clear and transparent glass. The starting materials used for the preparation of the glasses were analytical grade reagents (99.9% pure) of ZnO, ZnF_2, H_3BO_3 and TiO_2. Powders of these compounds taken into appropriate amounts (all in mol%) were thoroughly mixed in an agate mortar and afterwards were melted in a platinum crucible within the temperature range 1000–1050 °C in a PID temperature controlled furnace for about 1 h till a bubble free liquid was formed. The resultant bubble free melt was then poured on rectangular brass mold (containing smooth polished inner surface) kept at room temperature. The samples were subsequently annealed at 250 °C in another furnace and cooled to ambient temperature at the rate of about 1 °C/min. For the crystallization, the glass specimens were initially heated up to crystallization temperature 700–750 °C (identified from DSC traces) at the rate of 3 °C/min and then were held at the specified temperature for 72 h. After that the samples were cooled slowly (for about 3 h) to the offset temperature of the crystallization peak (to avoid cracks, voids due to subsequent sudden cooling) and then chilled in air to room temperature.

The samples synthesized were mechanically ground and polished to mirror-like surface with cerium oxide powder. The final dimensions of the samples used for the measurements were about $1.0 \times 1.0 \times 0.2\ cm^3$. Scanning electron microscopy studies were carried out on these samples to observe the crystallinity using HITACHI S-3400N Scanning Electron Microscope. The crystalline phases in the heat treated samples were identified using Rigaku D/Max ULTIMA III X-ray diffractometer with CuK_α radiation. The density of the glasses was determined with precision up to (± 0.0001) by the standard Archimedes' method using o-xylene (99.99% pure) as the buoyant liquid. The mass of the samples was measured with an accuracy of 0.1 mg using Ohaus digital balance Model AR2140 for evaluating the density. The refractive index (n) of the samples was measured at $\lambda = 589.3$ nm using Abbe refractometer with mono-bromo naphthalene as the contact layer situated between the glass and the refractometer prism to an accuracy of 0.001. The dielectric measurements were recorded using LF-impedance analyzer (Hewlett-Packard Model 4192A) in the frequency range 10^2–10^6 Hz and in the temperature range of 30–300 °C. The accuracy in the measurement of dielectric constant ε' is $\sim \pm 0.01$ and the dielectric loss ($\tan\delta$) is $\sim \pm 0.001$. The dielectric breakdown strength of all these glasses was determined at room temperature in air medium using a high a.c. voltage breakdown tester (ITL Model BOV-7, Hyderabad) operated with an input voltage of 230 V at frequency of 50 Hz. The details of other measurements viz., DSC, IR and optical absorption are similar to those reported in our earlier papers [20–21].

3. Results

From the measured values of the density and average molecular weight M of the samples, various other physical parameters such as titanium ion concentration N_i, mean titanium ion separation R_i, polaron radius R_p in $ZnO–ZnF_2–B_2O_3$:TiO_2 glass ceramic samples were evaluated and

Table 1
Physical Parameters of $ZnO-ZnF_2-B_2O_3$ glass ceramics doped with different concentration of TiO_2.

Sample	Density (g/cm^3)	Dopant ion conc. N_i ($\times 10^{20}$ ions/cm^3)	Inter ionic distance (Å)	Polaron radius (Å)	Refractive index (n)
TC_0	3.344	–	–	–	1.648
TC_1	3.345	2.48	7.38	2.97	1.652
TC_2	3.353	4.98	5.85	2.36	1.658
TC_3	3.355	7.47	5.11	2.06	1.663
TC_4	3.374	10.02	4.64	1.87	1.670
TC_5	3.378	12.54	4.30	1.73	1.675

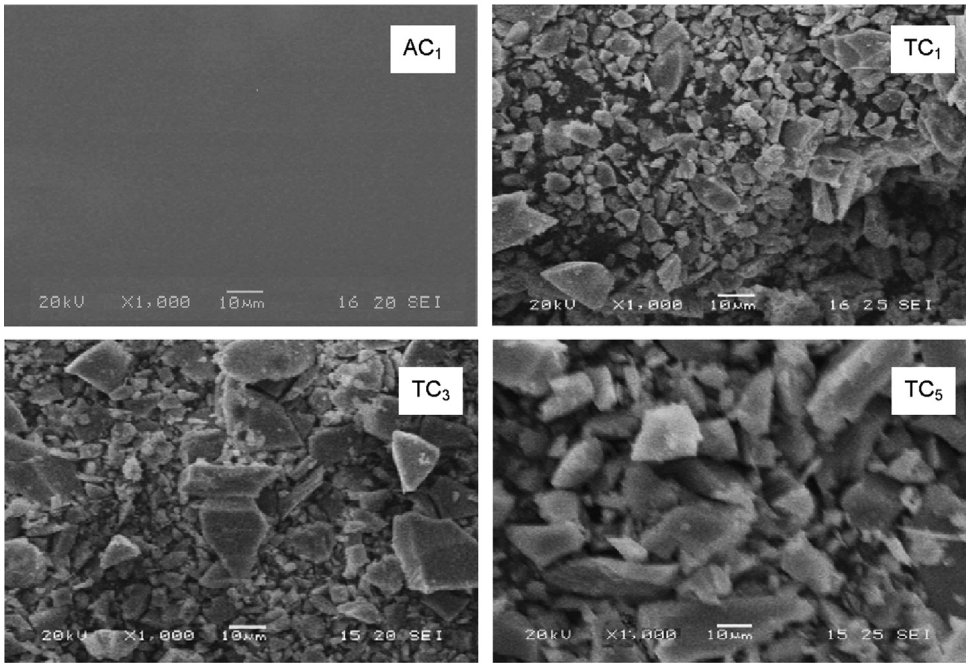

Fig. 1. SEM pictures of $ZnO-ZnF_2-B_2O_3$ glass ceramics doped with different concentration of TiO_2.

presented in Table 1. The density of the samples is observed to increase slightly with the concentration of TiO_2.

The scanning microscopy pictures for some of the crystallized samples are shown in Fig. 1. The pictures clearly indicate that the samples are embedded with well defined, randomly distributed crystals of different sizes (varying from 1 μm to 5 μm). The residual glass phase is acting as interconnecting zones among the crystallized areas, making the samples free of voids and cracks. The pictures further indicate a gradual increase in the volume fraction of crystallites in the samples with increasing concentration of TiO_2 indicating that TiO_2, enhances the phase separation tendency of various crystalline phases.

X-ray diffraction pattern for the $ZnO–ZnF_2–B_2O_3$ glass ceramic doped with 0.1 mol% of TiO_2 is shown in Fig. 2(a). The patterns exhibited peaks due to deflect crystal phases; some of them are $\alpha Zn(BO_2)_2$, $ZnTiO_3$, ZnO, Zn_2TiO_4, TiF_3, $TiOF_2$; the details JCPDS card numbers for these crystalline phases can be found in Ref. [22]. The XRD patterns for all the crystallized glasses are shown in Fig. 2(b). Most interestingly we have observed diffraction peaks with significant intensity and full width at half maximum due to $ZnTiO_3$ ($2\theta = 30.05$), Zn_2TiO_4 ($2\theta = 34.880$, 42.399, 61.795) and $TiOF_2$ ($2\theta = 23.662$, 48.144 and 54.463) crystal phases. This observation points out that part of titanium ions exist prevailingly in Ti^{4+} state even after crystallization. However, the intensity of these peaks is found to decrease with the increase of TiO_2 content. Diffraction peaks originating from TiF_3 crystal phase at about $2\theta = 22.919$, 46.902 and 52.463 are also observed in the pattern. The presence of such phases clearly suggests that a fraction of the titanium ions exists in Ti^{3+} valence state which may serve as a network modifier. The intensity of these peaks is found to increase with increasing of TiO_2 content.

DSC scans for $ZnO–ZnF_2–B_2O_3$:TiO_2 glass ceramic samples are shown in Fig. 3. The thermograms of all glass ceramic samples indicate presence of weak glass transitions with the inflection point situated between 575 and 620 °C, accompanied by the multiple exothermic peaks at the three steps of crystallization temperatures. From the measured values of T_g (inflection point), T_c (peak crystallization), the glass forming ability parameter ($T_c - T_g$), that give the information on the stability of the glass against devitrification for all the glass ceramics are presented in Table 2. The variation of ($T_c - T_g$) parameter exhibited a decreasing trend with the increasing TiO_2 content.

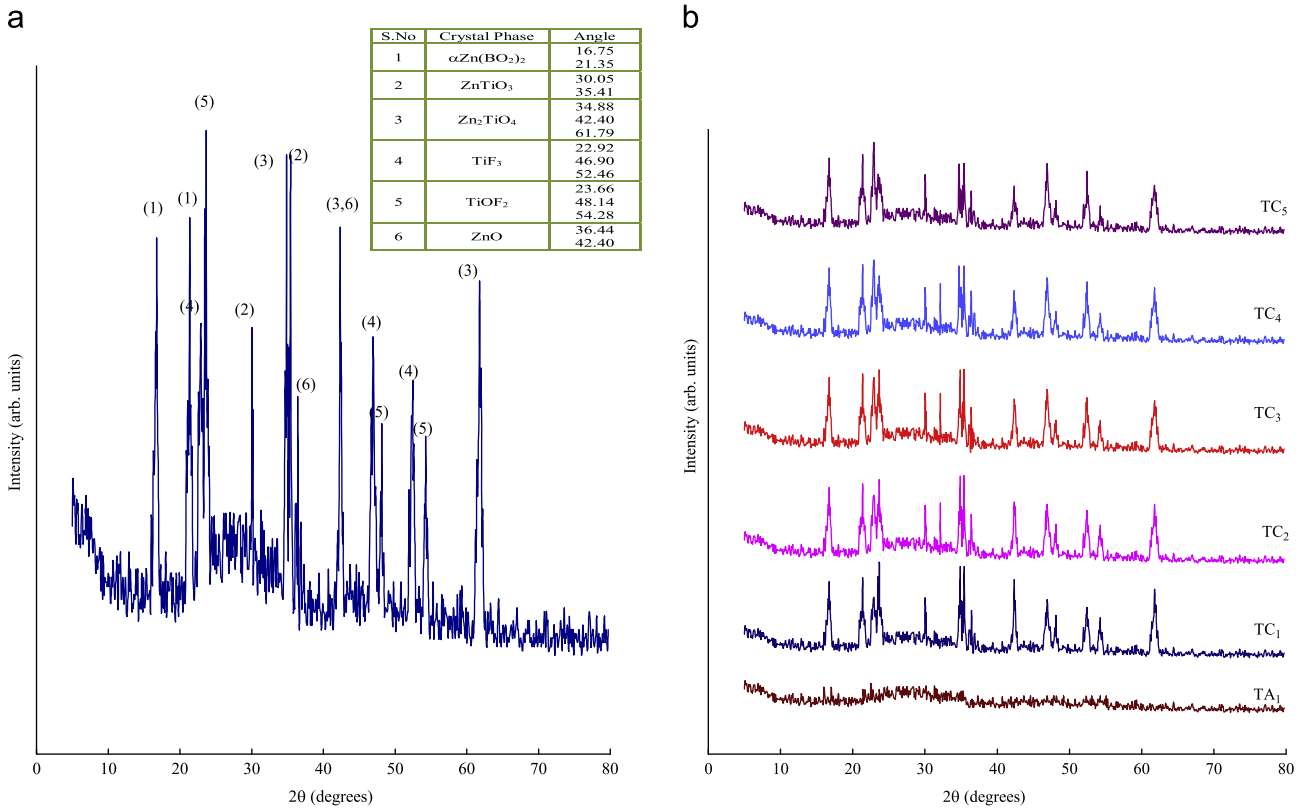

Fig. 2. (a) XRD patterns of $ZnO-ZnF_2-B_2O_3$: TiO_2 glass ceramic doped with 0.1 mol% of TiO_2. (b) XRD patterns of $ZnO-ZnF_2-B_2O_3$: TiO_2 glass ceramics doped with concentrations of TiO_2. For the sake of comparison, the XRD pattern of one of the pre-crystallized samples (TA_1) is also included.

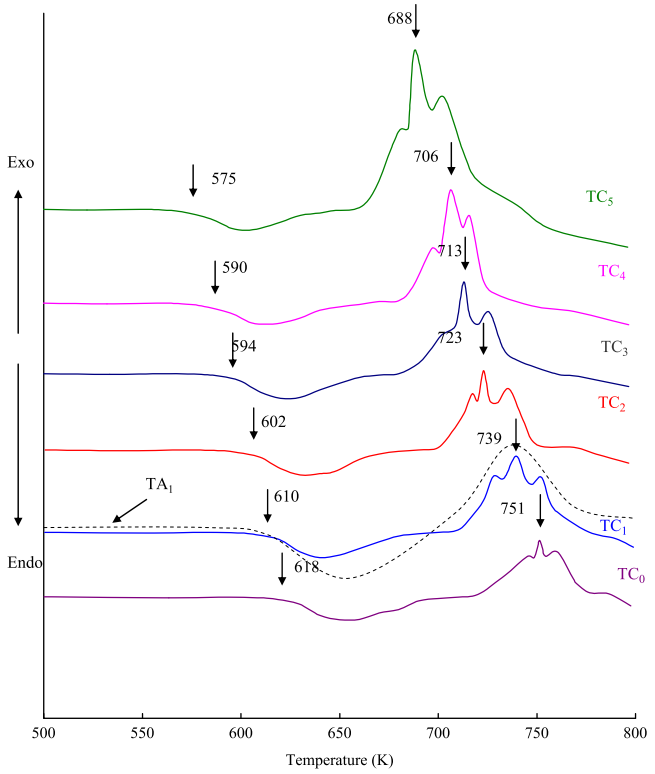

Fig. 3. DSC traces of $ZnO-ZnF_2-B_2O_3$: TiO_2 glass ceramics doped with concentrations of TiO_2.

Table 2
Summary of data on differential scanning calorimetric studies of $ZnO-ZnF_2-B_2O_3$ glass ceramics doped with different concentration of TiO_2.

Sample	Glass transition temperature (°C) (Inflection) (T_c)	Crystallization temperature (°C) (peak) (T_g)	T_c-T_g
TC_0	618	751	133
TC_1	610	739	129
TC_2	602	723	121
TC_3	594	713	119
TC_4	590	706	116
TC_5	575	688	113

For the sake of comparison the thermogram for one of the glass (pre-crystallized) samples (TA_1) is presented in the same figure. The figure indicates enthalpy increase, which is proportional to the area under crystallization peak when compared with that of corresponding crystallized sample.

Thus the results of SEM, XRD and DSC techniques clearly confirmed that the thermal treatment for prolonged times with different concentrations of TiO_2 caused the conversion of $ZnO–ZnF_2–B_2O_3$ glass samples into glass ceramics with entrenchment of fine crystals of different phases with Ti^{4+} and Ti^{3+} ions as components.

Fig. 4 presents optical absorption spectra of $ZnO–ZnF_2–B_2O_3$: TiO_2 glass ceramic samples recorded at room temperature in the spectral wavelength range 350–850 nm. The absorption edge

observed at 330 nm for TiO_2 free glass ceramic sample TC_0 exhibited spectrally red shift with the introduction of titanium oxide. The spectrum of the glass ceramic TC_1 exhibited two weak absorption bands at about 517 and 686 nm. When the concentration of TiO_2 is increased, the half width and intensity of these two bands are increased. The summary of the data on optical absorption spectra of these glasses is furnished in Table 3.

From the observed absorption edges, we have evaluated the optical band gap (E_o) of these samples by drawing Tauc plots [23] between $(\alpha\hbar\omega)^{1/2}$ vs. $\hbar\omega$ and $(\alpha\hbar\omega)^2$ vs. $\hbar\omega$ as per the equations

$$(\alpha\hbar\omega)^{1/2} = C(\hbar\omega - E_O) \quad (1a)$$

and

$$(\alpha\hbar\omega)^2 = C(\hbar\omega - E_O) \quad (1b)$$

which represent indirect and direct band gaps, respectively. Fig. 5 (a) and (b) represent such plots of all these glass ceramics. From the extrapolation of the linear portion of the curves, the values of both indirect and direct optical band gap (E_o) are determined and presented in Table 3; the value of E_o is found to decrease gradually from 3.41 eV (TC_0) to 2.95 eV (TC_5) with increase in the concentration of TiO_2.

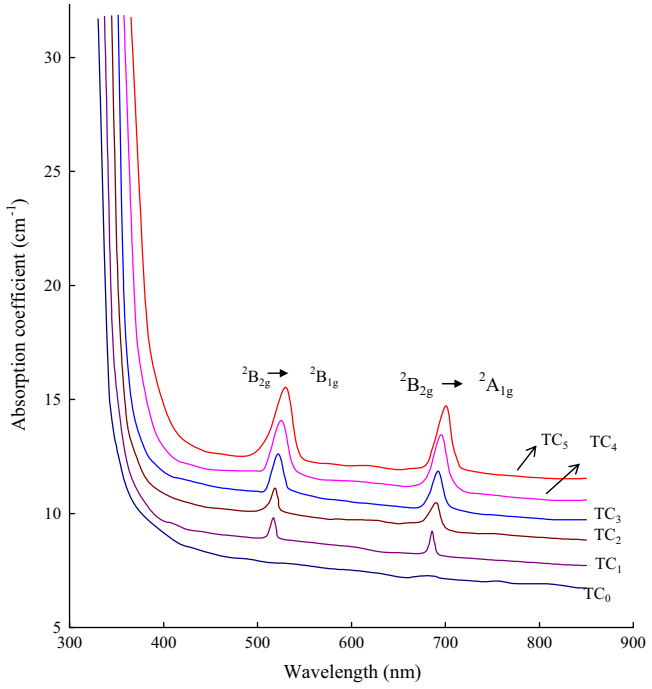

Fig. 4. Optical absorption spectra of $ZnO-ZnF_2-B_2O_3$: TiO_2 glass ceramics.

Infrared transmission spectra of TiO_2 free $ZnO–ZnF_2–B_2O_3$ glass ceramic exhibited two groups of bands: (i) in the region 1200–1600 cm^{-1}, (ii) in the region 800–1200 cm^{-1} and another band at about 690 cm^{-1} (Fig. 6). The second group of bands is attributed to the BO_4 units while the first group of bands is identified as being due to the stretching relaxation of the B–O bond of the trigonal BO_3 units and the band at 670 cm^{-1} is due to the bending vibrations of B–O–B linkages in the borate network [24,25]. Additionally, a band at about 488 cm^{-1} is also observed in the spectra of all the glasses; this band is attributed to the vibrations of ZnO_4 tetrahedral units [26]. The spectrum of the samples crystallized with (0.1 mol%) of TiO_2 exhibited two new bands in the regions 710–750 cm^{-1} and 625–640 cm^{-1}. These bands are identified as originated from Ti–O–Ti symmetric stretching vibrations of TiO_4 (tetrahedral) and due to the vibrations of TiO_6 (octahedral) units, respectively [27,28]. As the concentration of TiO_2 is increased, the band due TiO_6 (octahedral) grows gradually at the expense of TiO_4 tetrahedral band. In addition, with increase in the concentration of TiO_2, intensity of band due to BO_3 structural units is observed to increase at the expense of band due to BO_4 structural units. The summary of the data on various band positions of infrared spectra of the titled samples is given in Table 4.

Fig. 7 depicts the dispersion of dielectric constant, $\varepsilon'(\omega)$, vs. temperature, whereas Fig. 8 represents the same dependence at different temperatures of $ZnO–ZnF_2–B_2O_3$ glass crystallized with 0.3 mol% of TiO_2. The parameter, $\varepsilon'(\omega)$, increases with decreasing frequency. At larger frequency $\varepsilon'(\omega)$ approaches to achieve a constant value, $\varepsilon'_\infty(\omega)$ which normally results in a rapid polarization processes occurring in the glasses under applied field [29,30]. The variation of dielectric constant with temperature and frequency for all the other glass ceramics demonstrated similar behavior. However, for the sake of comparison, in the inset of Fig. 7 variation of dielectric constant with temperature measured at 1 kHz for $ZnO–ZnF_2–B_2O_3$ glasses crystallized with different concentrations of TiO_2 is presented. The variation exhibited increasing trend of dielectric constant with increasing TiO_2 content.

The dielectric loss, tan δ, dispersions at different temperature and vice versa at fixed temperature and different frequencies for the glass ceramic TC_4 are presented in Figs. 9 and 10, respectively. The loss dispersion curves have exhibited distinct

Table 3
Absorption band positions and optical band gaps of $ZnO-ZnF_2-B_2O_3$ glass ceramics doped with different concentration of TiO_2.

Sample	Cut-off wave length (nm)	Band positions		Optical band gap (eV)	Direct band gap (eV)
		$^2B_{2g} \rightarrow {}^2B_{1g}$	$^2B_{2g} \rightarrow {}^2A_{1g}$		
TC_0	330	–	–	3.41	3.60
TC_1	337	517	686	3.34	3.55
TC_2	344	518	689	3.25	3.47
TC_3	351	522	692	3.19	3.45
TC_4	358	525	698	3.02	3.33
TC_5	365	530	700	2.95	3.22

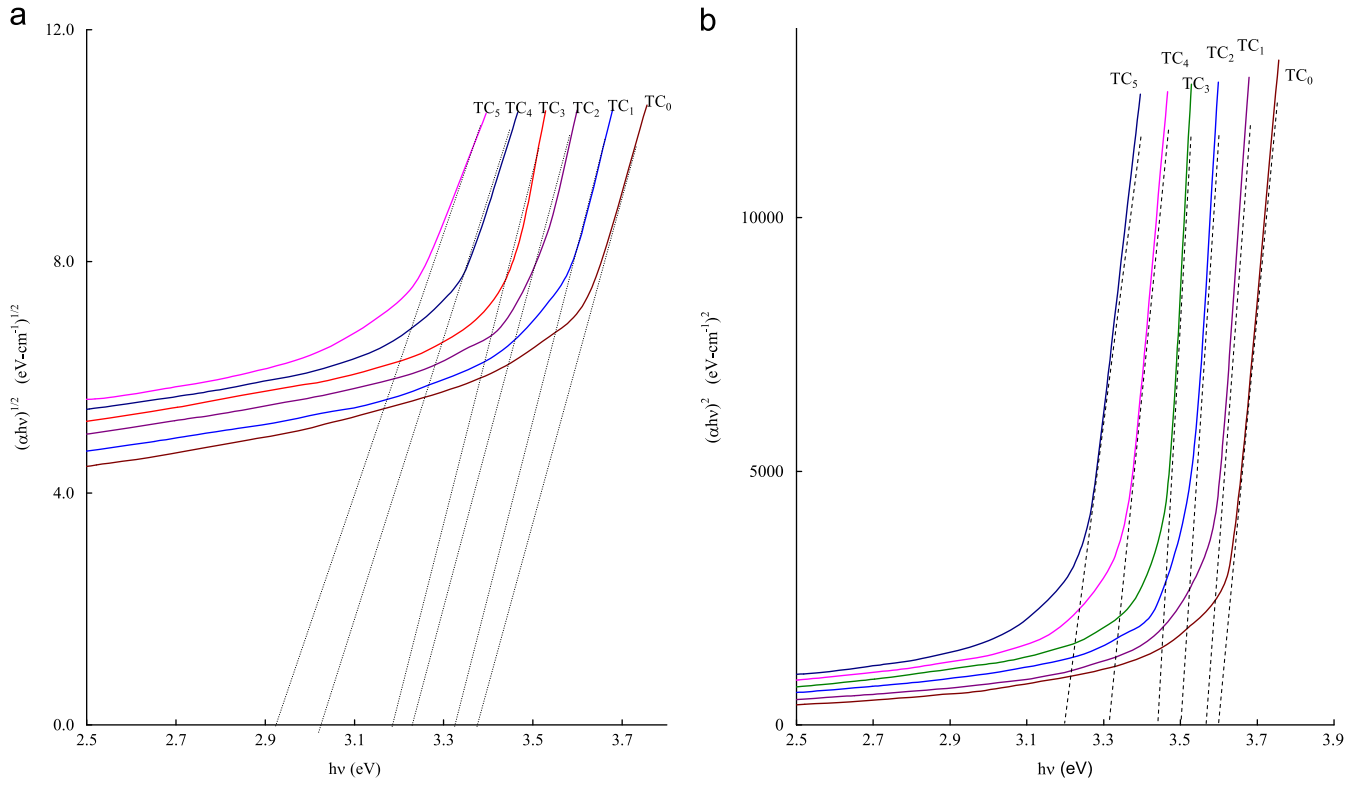

Fig. 5. (a) Tauc plots of $ZnO-ZnF_2-B_2O_3$: TiO_2 glass ceramics. (b). $(\alpha h\nu)^2$ vs. $h\nu$ plots of $ZnO-ZnF_2-B_2O_3$: TiO_2 glass ceramics.

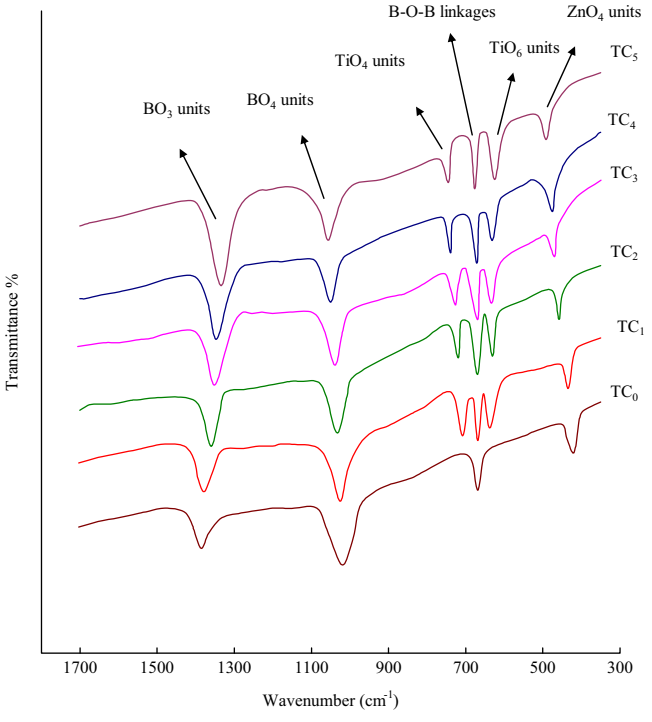

Fig. 6. IR Spectra of $ZnO-ZnF_2-B_2O_3$: TiO_2 glass ceramics.

maxima. With increasing temperature, the frequency maximum is shifted towards higher frequencies and with increasing frequency the temperature maximum is shifted towards higher temperatures. These observations confirm the relaxation character of dielectric loss peak for these glasses [29,31]. The origin of such variations of the dielectric loss dispersion vs. temperature is found to be similar for all the studied samples. However, the observations on dielectric loss variation with temperature for the samples crystallized with different concentrations of TiO_2 indicate an increase in the broadness and $(\tan\delta)_{max}$ of relaxation curves with the shifting of maxima towards lower temperature with increase in the concentration of TiO_2. From these curves, the effective activation energy W_d, for the dipoles is evaluated for the glasses crystallized with different concentrations of TiO_2 and presented in Table 5; the activation energy is found to be the lowest for the glass crystallized with 0.5 mol% of TiO_2 (Table 5). The a.c. conductivity σ_{ac} is calculated at different temperatures using the equation

$$\sigma_{ac} = \omega\varepsilon'(w)\varepsilon_o \tan\delta \quad (2)$$

(where ε_o is the vacuum dielectric constant) for different frequencies are evaluated. In Fig. 11 the plot of log σ_{ac} against $1/T$ for a glass ceramic (TC_5) at different frequencies is presented. The graph at lower temperatures especially at higher frequencies exhibited a plateau and at higher temperatures exhibited near linear tendency. The behavior of log σ_{ac} against $1/T$ for all other samples is found to be the similar. The conductivity is found to increase considerably with increase in the concentration of nucleating agent TiO_2 at any given frequency and temperature (inset (a) of Fig. 11). From these plots, the activation energy for the conduction in the high

Table 4
IR spectral band positions (in cm^{-1}) of $ZnO-ZnF_2-B_2O_3$ glass ceramics doped with different concentration of TiO_2.

Sample	Band positions			TiO_4 units	TiO_6 units	ZnO_4 units
	BO_3	BO_4	B–O–B			
TC_0	1385	1020	668	–	–	418
TC_1	1380	1025	668	709	637	433
TC_2	1360	1032	669	719	631	458
TC_3	1351	1038	670	726	633	469
TC_4	1346	1050	671	739	631	475
TC_5	1334	1058	676	744	625	492

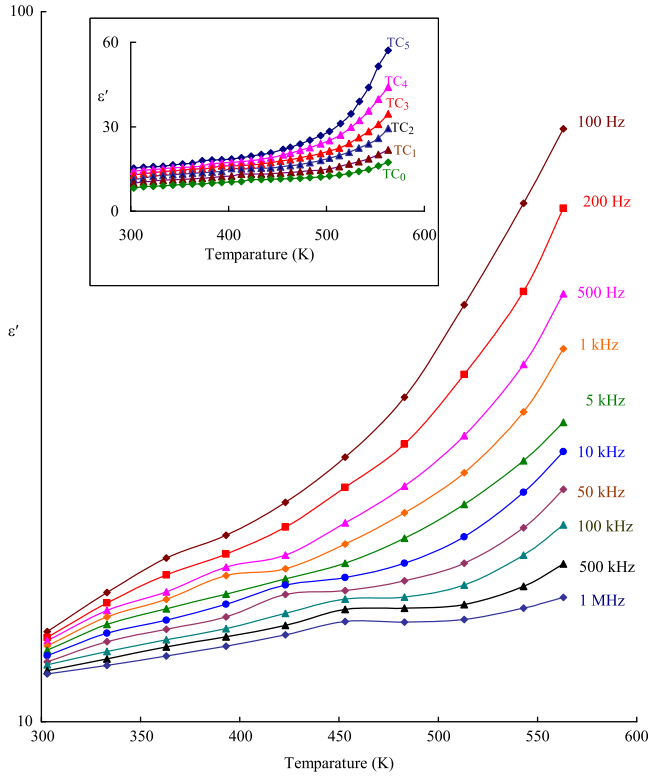

Fig. 7. Variation of dielectric constant $\varepsilon'(\omega)$ with temperature for the glass ceramic (TC_3) at different frequencies. Inset represents variation of dielectric constant $\varepsilon'(\omega)$ with temperature for different glass ceramics measured at 1 kHz.

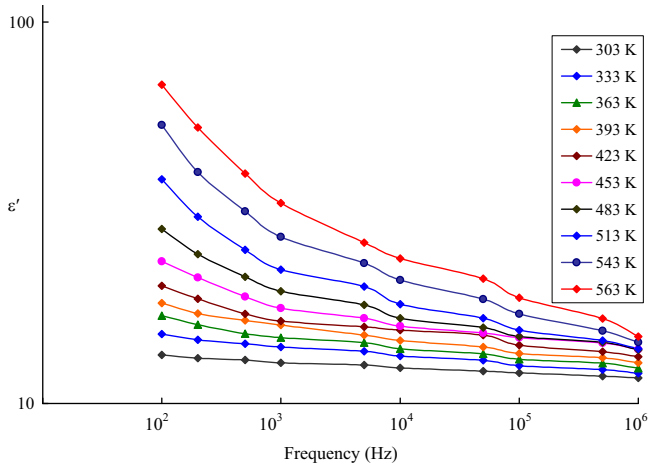

Fig. 8. Variation of dielectric constant $\varepsilon'(\omega)$ with frequency for the glass ceramic (TC_3) at different temperatures.

temperature region over which a near linear dependence of log σ_{ac} with $1/T$ could be observed is evaluated and presented in Table 5; this activation energy is also found to decrease gradually with increase in the concentration of the crystallizing agent (inset (a) of Fig. 11). The value of the dielectric breakdown strength is observed to decrease with the content of TiO_2 in bulk sample (Table 5).

4. Discussion

Among different constituents of $ZnO–ZnF_2–B_2O_3$: TiO_2 glass ceramic B_2O_3 is a strong glass former, when it is mixed with ZnO generally, tetrahedral boron entities dominate in the Zn-rich domain and form easily B–O–Zn bridges, whereas trigonal boron entities prevail in the borate-rich side. The highest stability occurs for fully polymerized glasses and can be related to the energetics of the reaction B–O–B+Zn–O–Zn=2(B–O–Zn) which also suggests that the B–O–Zn linkage is more stable relatively to the mixture of B–O–B and Zn–O–Zn linkages [32,33].

Titanium ions exist mainly in Ti^{4+} state in $ZnO–ZnF_2–B_2O_3$ glass network. Nevertheless, the reduction of Ti^{4+}–Ti^{3+} is quite possible during melting and crystallization processes of the glasses. Ti^{4+} ions occupy both tetrahedral and also substitutional octahedral sites as corner-sharing $[TiO_6]^{2-}$ units, whereas Ti^{3+} ions occupy only modifying positions and depolymerize the glass network [34]. TiO_4 and TiO_6 polyhedral of Ti^{4+} ions enter the glass network and form linkages of the type Zn–O–Ti and B–O–Ti.

The entry of TiO_2 into borate network may be presented as follows:

$$TiO_2 \equiv [TiO_{4/2}];$$
$$B_2O_3+2TiO_2+2O_2 \rightarrow 2[BO_{6/2}]^{3-}+[TiO_{4/2}]+[TiO_{6/2}]$$
$$B_2O_3+3TiO_2+2ZnO+3O_2 \rightarrow 2[BO_{6/2}]^{3-}+2[ZnO_{4/2}]^{+}+2[TiO_{4/2}]+[TiO_{6/2}]$$

The formation of $ZnTiO_3$, Zn_2TiO_4, $TiOF_2$ and TiF_3 crystalline phases detected from the XRD studies emphasizes that

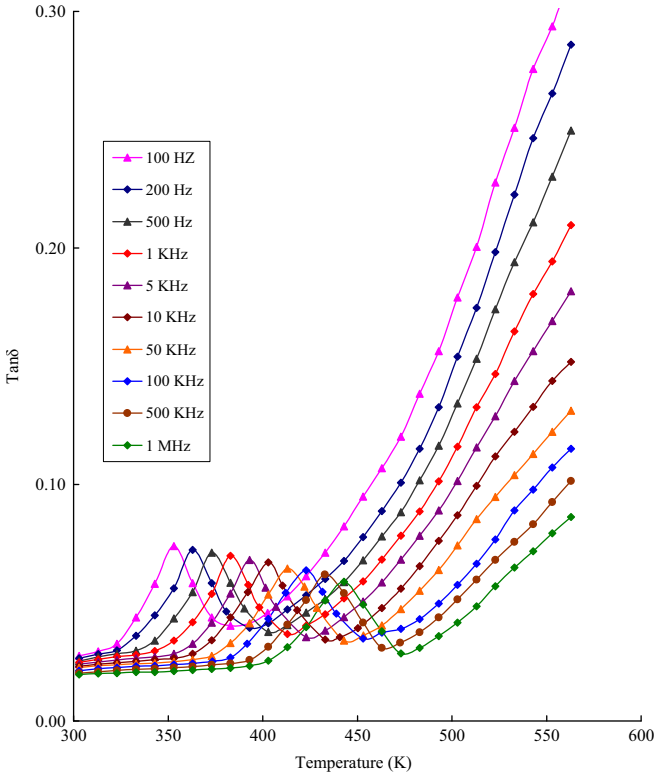

Fig. 9. Variation of dielectric loss tan δ with temperature for the glass ceramic (TC_4) at different frequencies.

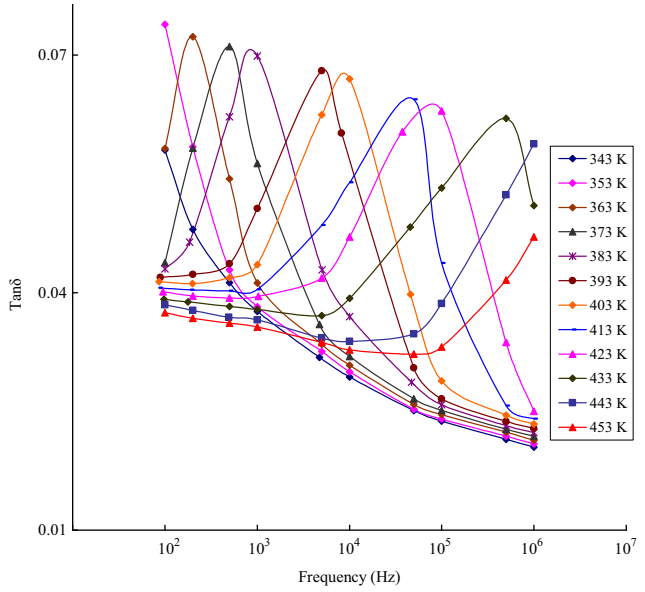

Fig. 10. Variation of dielectric loss tan δ with frequency for the glass ceramic (TC_4) at different temperatures.

titanium ions do exist in both Ti^{4+} and Ti^{3+} states in these glass ceramics. The gradual increase in the intensity of the diffraction peaks due to the TiF_3 crystallites with increase in the concentration of TiO_2 indicates increasing proportions of titanium ions in Ti^{3+} valence state.

The appearance of peaks due to different crystallization temperatures in the DSC pattern also suggests the presence of different phases of crystallization in the samples. The crystallization in the glass samples may take place following the surface and bulk nucleations. The apparent increase in value of enthalpy with increase in the nucleating agent suggests that the crystallization starts initially inside the material and expands to the surface gradually [35]. The real calorimetric exothermic effects (peaks) caused by crystallization in the amorphous sample have been suppressed by mutual movement and revolution (aggregation) of metal-oxygen octahedral (endothermic) in the plastic (flexible) phase, at temperature range which appear in the same temperature as the crystallization. This effects decreases actual enthalpy of crystallization, due to heating up to crystallization temperature (Fig. 3). During this process, the metal-oxygen bond length changes (may be that of Ti−O) as manifested by the other measurements.

The electronic configuration of Ti^{3+} ion is $3d^1$. In octahedral field or tetrahedral filed, the ground state ^2D of the $3d^1$ ion splits into ^2E and $^2T_2$ states. In the tetragonally distorted octahedral field, the $^2T_2$ state further splits into three $^2B_2$ (viz.$|xy\rangle$, $|yz\rangle$ and $|zx\rangle$) states, whereas the ^2E excited state splits into $A_1|3z^2-r^2\rangle$ and $B_1|x^2-y^2\rangle$ states by tetragonal distortion. For ions in tetragonally compressed octahedron, the ground state is $B_2|xy\rangle$. The bands observed in the optical absorption spectra at about 520 nm and 690 nm of the studied glass ceramics are identified as being due to $^2B_{2g}\rightarrow{}^2B_{1g}$ and $^2B_{2g}\rightarrow{}^2A_{1g}$ octahedral transitions of the Ti^{3+} (d^1) ions, respectively [36]. The observed gradual growth of these two bands with increase in the concentration of TiO_2 indicates that there is an increasing fraction of Ti^{4+} ions that have been reduced in to Ti^{3+} ions. Further, we have noticed a gradual decrease in the optical activation energy associated with these bands with increase in the concentration of TiO_2. For example, the excitation energy associated with $^2B_{2g}\rightarrow{}^2B_{1g}$ transition is decreased from 2.40 to 2.34 eV when the concentration of TiO_2 is varied from 0.1 to 0.5 mol%. This is clearly a characteristic feature for inter-valence transfer or a polaronic type of absorption. It means that the associated electrons are trapped at shallow sites within the main band gap and as a consequence possess smaller effective wave-function radii. This kind of situation is only possible if the local potential fluctuation may be neglected with respect to transfer integral, j. A small overlap between electronic wavefunctions (corresponding to adjacent sites) due to strong local disorder is contributive to polaron formation. So within a framework of polaronic model, the electron delivered by the impurity atom at Ti^{4+} site converts this one into a lower valence state Ti^{3+}. Afterwards the trapped electron at this Ti^{3+} site is transferred to the neighboring new Ti^{4+} site by absorbing a photon quantum. Thus the optical absorption in the glass samples is dominated by polaronic transfer between the Ti^{3+} and Ti^{4+} species [20,37].

The validity of the Eqs. 1(a and b) related to optical band gap points out that the band gap is caused by amorphous optical absorption edge as well as indirect band gap (i.e. the transitions in the different points of the Brillouin zone) valid

Table 5
Summary data on dielectric studies of $ZnO-ZnF_2-B_2O_3$ glass ceramics doped with different concentration of TiO_2.

Sample	Temp. region of relaxation (K)	A.E. for conduction (eV)	A.E. for dipoles (eV)	Exponent (s)	N(E_F) ($\times 10^{21}$, eV^{-1}/cm^3) (± 0.01)	Breakdown strength (kV/cm)
TC_0	395–482	0.55	1.44	0.81	3.40	12.92
TC_1	386–474	0.51	1.41	0.83	4.35	12.27
TC_2	377–468	0.48	1.37	0.86	6.03	11.85
TC_3	365–452	0.43	1.32	0.89	7.58	11.32
TC_4	353–446	0.41	1.29	0.91	9.51	10.97
TC_5	345–440	0.36	1.26	0.92	11.35	10.54

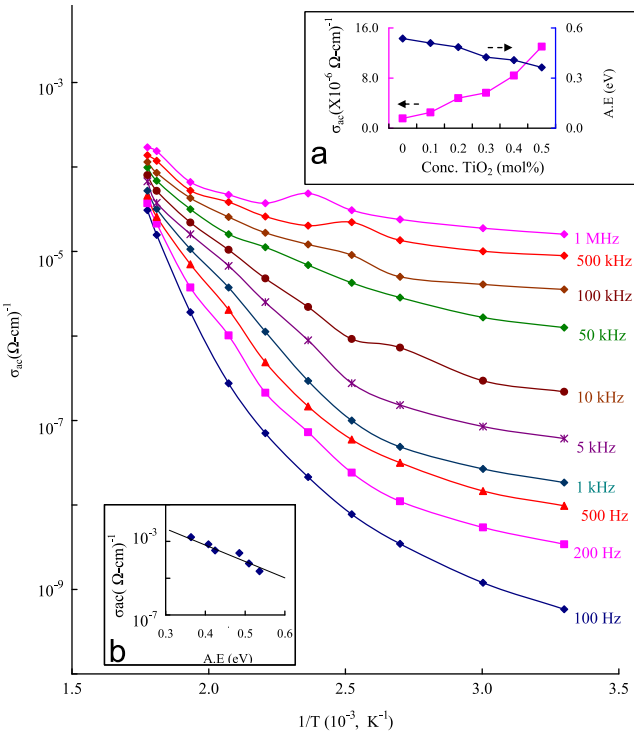

Fig. 11. Variation of a.c. conductivity with $1/T$ for the glass ceramic (TC_5) at different frequencies. Inset (a) shows the variation of a.c. conductivity and activation energy with concentration of crystallizing agent TiO_2 and (b) shows the variation of a.c. conductivity with activation energy.

for crystalline materials. This confirms the fact that the studied materials are formed by direct and partial indirect transitions between the valence band and the conduction band.

The gradual increase in the concentration of Ti^{3+} ions causes a creation of large number of donor centers; subsequently, the excited states of localized electrons originally trapped on Ti^{3+} sites begin to overlap with the empty 3d state on the neighboring Ti^{4+} sites. As a result, the impurity band becomes more extended into the main band gap. This development may cause a shift of the absorption edge to the lower energy (Table 3) which leads up to a significant shrinkage in the band gap with increase in the concentration of TiO_2, as observed.

The gradual increase in the intensity of the bands due to BO_3 and TiO_6 structural units (at the expense of the bands due to BO_4 and TiO_4 structural units) in the IR spectra with increase in the concentration of the nucleating agent TiO_2 also supports the view point that there is a gradual increase in the degree of disorder in the glass network. This is once again a manifestation of higher concentration of Ti^{3+} ions that act as modifiers in the samples crystallized with higher contents of TiO_2.

The observed increase of $\varepsilon'(\omega)$ at higher temperatures and at lower frequency can be attributed to the bulk surface charge polarization of the glass ceramics resulted from the presence of metallic electrodes accumulated with charge species. The behavior of frequency dependence of dielectric permittivity is related to the application of the field which favours electron hopping between two different sites in the glasses. This also leads to an increase of the electronic component in dielectric constant dispersion. At higher frequency, the charge carriers will no longer be able to rotate sufficiently rapidly, so their oscillation will begin to lay behind this field leading to a decrease of dielectric permittivity, $\varepsilon'(\omega)$.

The increase of TiO_2 content up to 0.5 mol% in the glass network causes increase of permittivity, $\varepsilon'(\omega)$, at any frequency and temperature. This observation supports an increase in degree of disorder in the network with increasing content of the crystallizing agent TiO_2 [21,38]. From the optical absorption studies it is evident that with the gradual increase of TiO_2 there is a continuous fractional increase in the concentration of Ti^{3+} ions. The Ti^{3+} ions, similarly to Zn^{2+} ions, act as modifiers and create dangling bonds and non-bridging oxygen ions by disrupting B–O–B and B–O–Zn linkages. Such produced defects create an easy pathways for the migration of charge carriers that would enhance the space charge polarization causing an increase $\varepsilon'(\omega)$ with the increase of TiO_2 content up to 0.5 mol% [39–41].

The way the dielectric loss varies with temperature indicates that there is a spreading of relaxation times for the studied glass ceramic samples. Such spreading is possibly due to the coupling of individual relaxation processes, one site needing to relax before the other can do so. Even if each relaxation site has the same value of τ the coupling between them ensures that the time domain is effectively stretched leading to the spreading of relaxation times as observed [42,43]. The possible contributors to the dipolar effects in addition to the octahedral complexes of Zn^{2+} ions are the complexes of Ti^{3+} ions [44]. The decrease of activation energy for dipoles and also the

relaxation time with increase in the content of TiO_2 (Table 5), suggests increasing degree of freedom for dipoles to orient in the field direction in the network.

When a plot is made between log σ_{ac} vs. activation energy for conduction, a near-linear relationship is observed (inset (b) of Fig. 11). This observation suggests that the conductivity enhancement is directly related to the thermally stimulated mobility of the charge carriers at higher temperatures. The glasses under study are expected to exhibit mixed, ionic and polaronic, conductivity. Generally, electronic conduction is due to the polaron hopping between Ti^{3+} and Ti^{4+} ions, whereas ionic conduction is predominately due to migration of zinc ions [45].

For the studied glasses, a.c. conductivity increases with increasing content of TiO_2. The possible explanation for such a behavior is that with the gradual increase of TiO_2 content, there is a growing presence of Ti^{3+} ions that act as modifiers and enhance the concentration of dangling bonds in the glass network. This in turn causes a decrease in the electrostatic binding energy and the strain energy for the easy passage of zinc ions, which consequently leads to a substantial decrement in the jump distance for these ions. Such behavior is in good agreement with the observed decrease in activation energy for conduction. To be more specific, the decrease in activation energy and increase in the conductivity with increasing TiO_2 content are caused by two mechanisms. One is related to significant ionic contribution due to easy pathways for zinc ions and second one is caused by an increase of $Ti^{3+}-Ti^{4+}$ pairs since there is a gradual increase of TiO_2 content and Ti^{3+} ions concentration. Generally, the high fragmentation of the zinc borate in the present compositions due to higher Ti^{3+} ions concentration can promote this mechanism, by stabilizing temporary sites with interstitial rather than vacancy character, through local distortion of the network.

The real part dispersion for a.c. conductivity is usually described by power law dependence $\sigma(\omega) \propto \omega^s$ when the mean square displacement of ions is small and the ion transport is characterized by the non-random forward–backward hopping process. The variation of the exponent (obtained by plotting log $\sigma(\omega)$ vs. ω) is found to increase with increasing the concentration of TiO_2 (Table 5) suggesting that dimensionality of conducting space increases with the content of TiO_2 [46–48].

The a.c. conductivity in the low temperature region (near plateau region) can be understood following the quantum mechanical tunneling model. Based on Austin and Mott's model (quantum mechanical tunneling model) [49], the density of defect energy states near the Fermi level, $N(E_F)$, at nearly temperature independent region of the conductivity (low temperature) is evaluated using

$$\sigma(\omega) = (\pi/3)e^2 k_B T[N(E_F)]^2(\alpha')^{-5} w(\ln(\nu_o/\omega))^4 \quad (3)$$

In Eq. (3), α' is the electronic wave function decays constant, ν_0 ($\sim 5 \times 10^{12}$ Hz) is the phonon frequency. The value of $N(E_F)$ was calculated at a frequency of 1 kHz, $T = 370$ K, taking $\alpha' = 0.50$ (Å)$^{-1}$ (obtained by plotting log σ_{ac} against R_i), and the values obtained are presented in Table 5. The value of $N(E_F)$ is found to increase with increasing the concentration of TiO_2 thus supporting view point that there is an increasing concentration of defect energy states with increase in the concentration of TiO_2 supporting the view point that there is a gradual increase in the concentration of Ti^{3+} ions that increase degree of disorder in the glass ceramic network.

The specific dielectric loss i.e., the loss per unit volume of the dielectric when placed under an alternating electric field is given by [50]

$$\rho_l = E^2 \omega \varepsilon'(\omega) \varepsilon_o \tan\delta \; W/m^3 \quad (4)$$

Eq. (4) indicates the specific dielectric loss is proportional to $\varepsilon'(\omega)\tan\delta$ of the sample. The dielectric breakdown strength is in fact inversely proportional to the specific dielectric loss. The measurements on dielectric properties of the titled samples exhibited increase of $\varepsilon'(\omega')\tan\delta$ with the concentration of TiO_2.

The observations on breakdown strengths of $ZnO–ZnF_2–B_2O_3$ glass ceramics, as mentioned earlier, indicated decreasing trend with the concentration of nucleating agent. This is well in accordance with the observed variation of the specific dielectric loss with the concentration of TiO_2. Thus the experiments on the dielectric breakdown strength of $ZnO–ZnF_2–B_2O_3$ ceramics reveal that there is an increase in the disorderliness in the samples with increase in the concentration of TiO_2 possibly due to increase in proportion of Ti^{3+} ions that act as modifiers.

5. Conclusions

$ZnO–ZnF_2–B_2O_3$ glasses doped with different concentrations of TiO_2 were synthesized and subsequently crystallized. The characterization of the samples by SEM, XRD and DSC techniques indicated that the samples contain well defined and randomly distributed grains of different crystalline phases. The XRD studies revealed that the samples were embedded with crystalline phases like $ZnTiO_3$, Zn_2TiO_4, $TiOF_2$, TiF_3 in which titanium ions exist Ti^{4+} and Ti^{3+} states. The IR spectral studies have indicated that the glass ceramic samples contains various structural units with the linkages of the type B–O–B, Zn–O–Zn, B–O–Zn, the increasing content of TiO_2 in the glass ceramics seemed to have weakened such linkages. The analysis of the results of optical absorption, the studied glass ceramics have indicated that a considerable proportion of titanium ions do exist in Ti^{3+} state in addition to Ti^{4+} state especially in the samples crystallized with higher mol% of TiO_2.

The variations of dielectric constant, $\varepsilon'(\omega)$, and loss, tan δ, with temperature have been analyzed on the basis of dielectric polarization. The frequency and temperature dependence of the dielectric loss parameters have exhibited relaxation character. The relaxation effects have been attributed to complexes of Zn^{2+} and Ti^{3+} ions. The observed increase in the electrical conductivity and decrease in the activation energy with increase in the concentration of the crystallizing agent (TiO_2) is attributed to two effects. One is due to the contribution of polaron $Ti^{3+}–Ti^{4+}$ pairs and the other is related to the significant ionic contribution due to an increase in the concentration of dangling bonds which leads to the substantial decrement in jump distance for zinc ions.

References

[1] L.R. Pinckney, Transparent glass ceramics based on ZnO crystals, Physics and Chemistry of Glasses—European Journal of Glass Science and Technology Part B 47 (2006) 127–130.

[2] A. Miguel, R. Morea, J. Gonzalo, M.A. Arriandiaga, J. Fernandez, R. Balda, Near-infrared emission and upconversion in Er^{3+}-doped TeO_2–ZnO–ZnF_2 glasses, Journal of Luminescence 140 (2013) 38–44.

[3] H. Ticha, M. Kincl, L. Tichy, Some structural and optical properties of (Bi_2O_3) $x(ZnO)$ $60-x(B_2O_3)_{40}$ glasses, Materials Chemistry and Physics 138 (2013) 633–639.

[4] T. Shinoda, M. Wakitani, T. Nanto, N. Awaji, S. Kanagu, Development of panel structure for a high-resolution 21-in-diagonal full-color surface-discharge plasma display panel, Electron Devices 47 (2000) 77–81.

[5] Fang-Hsing Wang, Hung-Peng Chang, Chih-Chung Tseng, Chia-Cheng Huang, Effects of H_2 plasma treatment on properties of ZnO:Al thin films prepared by RF magnetron sputtering, Surface and Coatings Technology 205 (2011) 5269–5277.

[6] H. Yamasaki, K. Minato, D. Nezaki, T. Okamoto, A. Kawamoto, M. Takata, Photoluminescence of zinc oxide crystals synthesized on zinc wire by electric current heating method, Solid State Ionics 172 (2004) 349–352.

[7] N. Saito, H. Haned, T. Skiguchi, N. Ohashi, I. Sakaguchi, K. Koumoto, Low temperature fabrication of light-emitting zinc oxide micropatterns using self-assembled monolayers, Advanced Materials 14 (2002) 418–421.

[8] B.L. Zhu, C.S. Xie, D.W. Zeng, W.L. Song, A.H. Wang, Investigation of gas sensitivity of Sb-doped ZnO nanoparticles, Materials Chemistry and Physics 89 (2005) 148–153.

[9] S.S.A. Qazvini, Z. Hamnabard, Z. Khalkhali, S. Baghshahi, A. Maghsoudipour, Photoluminescence and microstructural properties of SiO_2–ZnO–B_2O_3 system containing TiO_2 and V_2O_5, Journal of Ceramics International 1 (38) (2012) 1663–1670.

[10] I.A. Bondar, N.A. Toropov, in: E.A. Porai-Koshits (Ed.), The Structure of Glass, vol. 3, Consultants Bureau, New York, 1964, p. 35.

[11] C. Lakshmikanth, B.V. Raghavaiah, N. Veeraiah, Optical absorption, fluorescence and thermoluminescence properties of ZnF_2–MO–TeO_2 (MO=ZnO, CdO and PbO) glasses doped with Er^{3+} ions, Journal of Luminescence 109 (2004) 193–205.

[12] D.K. Durga, N. Veeraiah, Dielectric dispersion in ZnF_2–Bi_2O_3–TeO_2 glass system, Journal of Materials Science 36 (2001) 5625–5632.

[13] T. Satyanarayana, M.A. Valente, G. Nagarjuna, N. Veeraiah, Spectroscopic features of manganese doped tellurite borate glass ceramics, Journal of Physics and Chemistry of Solids 74 (2013) 229–235.

[14] N. Dai, H. Luan, Z. Liu, Y. Sheng, J. Peng, Z. Jiang, H. Li, L. Yang, J. Li, Broadband NIR luminescence of Bi-doped Li_2O–Al_2O_3–SiO_2 glass ceramics, Journal of Non-Crystalline Solids 358 (2012) 2970–2973.

[15] P. Srinivasa Rao, P.M. Vinaya Teja, A.Ramesh Babu, C.h. Rajyasree, D. Krishna Rao, Influence of molybdenum ions on spectroscopic and dielectric properties of ZnF_2–Bi_2O_3–P_2O_5 glass ceramics, Journal of Non-Crystalline Solids 358 (2012) 3372–3381.

[16] Z. Hou, Z. Xue, S. Wang, Synthesis and spectroscopic properties of Er^{3+}-doped CaF_2 nanocrystals in transparent oxyfluoride tellurite glass–ceramics, Journal of Alloys and Compounds (2012) 109–112.

[17] N. Shimoji, T. Hashimoto, H. Nasu, K. Kamiya, Non-linear optical properties of Li_2O–TiO_2–P_2O_5 glasses, Journal of Non-Crystalline Solids 324 (2003) 50–57.

[18] A. Shaim, M. Et-tabirou, Role of titanium in sodium titanophosphate glasses and a model of structural units, Materials Chemistry and Physics 80 (2003) 63–67.

[19] R.K. Brow, D.R. Tallant, W.L. Warren, A. McIntyre, D.E. Day, Spectroscopic studies of the structure of titanophosphate and calcium titanophosphate glasses, Physics and Chemistry of Glasses 38 (1997) 300–306.

[20] N. Narasimha Rao, I.V. Kityk, V. Ravi Kumar, Ch. Srinivasa Rao, M. Piasecki, P. Bragiel, N. Veeraiah, Dc field induced optical effects in ZnF_2–PbO–TeO_2:TiO_2 glass ceramics, Ceramics International 38 (2012) 2551–2562.

[21] T. Srikumar, I.V. Kityk, Ch. Srinivasa Rao, Y. Gandhi a, M. Piasecki, P. Bragiel, V. Ravi Kumar, N. Veeraiah, Photostimulated optical effects and some related features of CuO mixed Li_2O–Nb_2O_5–ZrO_2–SiO_2 glass ceramics, Ceramics International 37 (2011) 2763–2779.

[22] Powder Diffraction File, Alphabetical Index, Inorganic Compounds, JCPDS, International Centre for Diffraction Data, Newtown Square, PA, 2003.

[23] K. Morigaki, Physics of Amorphous Semiconductors, World Scientific, Singapore, 1999 140.

[24] K.J. Rao, Structural Chemistry of Glasses, Elsevier, Amsterdam, 2002.

[25] W. Vogel, Glass Chemistry, Springer, Berlin, 1994.

[26] G. Naga Raju, M. Srinivasa Reddy, K.S.V. Sudhakar, N. Veeraiah, Spectroscopic properties of copper ions in ZnO–ZnF_2–B_2O_3 glasses, Optical Materials 29 (2007) 1467–1474.

[27] Hui-Fen Wu, Chung-cheng Lin, Pouyan Shen, Structure and dissolution of CaO–ZrO_2–TiO_2–Al_2O_3–B_2O_3–SiO_2 glass (II), Journal of Non-Crystalline Solids 209 (1997) 76–86.

[28] G. Murali Krishna, N. Veeraiah, N. Venkatramaiah, R. Venkatesan, Induced crystallization and physical properties of Li_2O–CaF_2–P_2O_5:TiO_2 glass system: Part II. Electrical, magnetic and optical properties, Journal of Alloys and Compounds 450 (2008) 486–493.

[29] T. Komatsu, N. Soga, M. Kunugi, ESR study of $NiFe_2O_4$ precipitation process from silicate glasses, Journal of Applied Physics 50 (1979) 6469–6474.

[30] K. Srilatha, K. Sambasiva Rao, Y. Gandhi, V. Ravikumar, N. Veeraiah, Fe concentration dependent transport properties of LiI–AgI–B_2O_3 glass system, Journal of Alloys and Compounds 507 (2010) 391–398.

[31] T. Srikumar, C.h. Srinvasa Rao, Y. Gandhi, N. Venkatramaiah, V. Ravikumar, N. Veeraiah, Microstructural, dielectric and spectroscopic properties of Li_2O–Nb_2O_5–ZrO_2–SiO_2 glass system crystallized with V_2O_5, Journal of Physics and Chemistry of Solids 72 (2011) 190–200.

[32] E.T.Y. Lee, E.R.M. Taylor, Compositional effects on the optical and thermal properties of sodium borophosphate glasses, Journal of Physics and Chemistry of Solids 66 (2005) 47–51.

[33] R.K. Brow, An XPS study of oxygen bonding in zinc phosphate and zinc borophosphate glasses, Journal of Non-Crystalline Solids 194 (1996) 267–273.

[34] B.V.R. Chowdari, G.V. Subba Rao, G.Y.H. Lee, X.P. Sand, XPS and ionic conductivity studies on Li_2O–Al_2O_3–(TiO_2 or GeO_2)–P_2O_5 glass–ceramics, Solid State Ionics 136 (2000) 1067–1075.

[35] F. Branda, A. Buri, A. Marotta, S. Saiello, Kinetics of crystal growth in, $Na_2O \cdot 2SiO_2$ glass. A DTA study, Thermochimica Acta 77 (1984) 13–18.

[36] A. Aboukais, L.D. Bogomolova, A.A. Deshkovskaya, V.A. Jachkin, N.A. Krasil Nikova, S.A. Prushinsky, O.A. Trul, S.V. Stefanovsky, E.A. Zhilinskaya, EPR of silica and fluoride glasses implanted with titanium and zirconium, Optical Materials 19 (2002) 295–306.

[37] B.V.R. Chowdari, P. Pramoda Kumari, Studies on $Ag_2O \cdot M_xO_y \cdot TeO_2$ (M_xO_y=WO_3, MoO_3, P_2O_5 and B_2O_3) ionic conducting glasses, Solid State Ionics 113 (1998) 665–675.

[38] Y. Gandhi, N. Krishna Mohan, N. Veeraiah, Role of nickel ion coordination on spectroscopic and dielectric properties of ZnF_2–As_2O_3–TeO_2:NiO glass system, Journal of Non-Crystalline Solids 357 (2011) 1193–1202.

[39] N. Krishna Mohan, G. Sahaya Baskaran, N. Veeraiah, Dielectric and spectroscopic properties of PbO–Nb_2O_5–P_2O_5:V_2O_5 glass system, Physica Status Solidi A 203 (2006) 2083–2102.

[40] A. Mogus-Milankovic, V. Licina, S.T. Reis, D.E. Day, Electronic relaxation in zinc iron phosphate glasses, Journal of Non-Crystalline Solids 353 (2007) 2659–2666.

[41] M. Srinivasa Reddy, S.V.G.V.A. Prasad, N. Veeraiah, Valence and coordination of chromium ions in ZnO–Sb_2O_3–B_2O_3 glass system by means of spectroscopic and dielectric relaxation studies, Physica Status Solidi A 204 (2007) 816–832.

[42] V. Ličina, A. Moguš-Milanković, S.T. Reis, D.E. Day, Electronic conductivity in zinc iron phosphate glasses, Journal of Non-Crystalline Solids 353 (2007) 4395–4399.

[43] S.R. Elliott, Physics of Amorphous Materials, Longman Science and Technology, Essex, 1990.

[44] S.V.G.V.A. Prasad, G. Sahaya Baskaran, N. Veeraiah, Spectroscopic, magnetic and dielectric investigations of $BaO–Ga_2O_3–P_2O_5$ glasses doped by Cu ions, Physica Status Solidi A 202 (2005) 2812–2828.
[45] N.S.V. Narayanan, B.V. Ashokraj, S. Sampath, Ambient temperature, zinc ion-conducting, binary molten electrolyte based on acetamide and zinc perchlorate: application in rechargeable zinc batteries, Journal of Colloid and Interface Science 342 (2010) 505–509.
[46] R.G. Palmer, D.L. Stein, E. Abrahamy, P.W. Andersons, Models of hierarchically constrained dynamics for glassy relaxation, Physical Review Letters 53 (1984) 958–961.
[47] D.L. Sidebottom, Dimensionality dependence of the conductivity dispersion in ionic materials, Physical Review Letters 83 (1999) 983–986.
[48] S. Bhattacharya, A. Ghosh, Conductivity spectra in fast ion conducting glasses: mobile ions contributing to transport processes, Physical Review B 70 (2004) 172203.
[49] I.G. Austin, N.F. Mott, Polarons in crystalline and non-crystalline materials, Advances in Physics 18 (1969) 41–102.
[50] B. Tareev, Physics of Dielectric Materials, Mir Publishers, Moscow, 1979.